From forward modelling of MT phases over 90° towards 2D anisotropic inversion

X. Chen[1,2], U. Weckmann[1], K. Tietze[1,3]

[1]Helmholtz Centre Potsdam - German Research Center for Geosciences,Germany

[2]University of Potsdam, Institute of Geosciences, Germany

[3]Free University of Berlin, Institute of Geological Sciences, Germany

xiaoming@gfz-potsdam.de, uweck@gfz-potsdam.de, ktietze@gfz-potsdam.de

Abstract

Within the framework of the German - South African geo-scientific research initiative Inkaba yeAfrica several magnetotelluric (MT) field experiments were conducted along the Agulhas-Karoo Transect in South Africa. This transect crosses several continental collision zones between the Cape Fold Belt, the Namaqua Natal Mobile Belt and Kaapvaal Craton. Along the profile we can identify areas ($> 10\,km$) with phases over 90°. This phenomenon usually occurs in presence of electrical anisotropy. Due to the dense site spacing we are able to observe this behaviour consistently at several sites.

In this presentation we focus on the profile section between Prince Albert and Mosselbay. With isotropic 2D inversion we are able to explain most features in the MT data but not the abnormal phase behavior. With several anisotropic forward modelling studies we have tested the influence of anisotropy parameters on the MT responses. In a first step we use simple 2D models with embedded zones of electrical anisotropy to get a basic understanding of anisotropic responses. In a second step isotropic 2D inversion results serve as background models in which we included anisotropic zones, e.g. to fit the abnormal phase curves. These resolution tests are necessary and important for the future development of a 2D inversion with spatially constraint anisotropy.

1 Introduction

For a 2D geoelectric model with a finite system of homogeneous, but generaly anisotropic blocks the electrical conductivity is a tensor instead of a scalar quantity. It is symmetric and positive-definite. Due to its symmetry the conductivity tensor $\widehat{\sigma}$ within each layer of model can be diagonalized and expressed by three principal conductivities σ_1, σ_2, σ_3 and a rotation matrix, which can be decomposed into three elementary Euler's rotations α_S, α_D, α_L respectively.

$$
\widehat{\sigma} = \begin{pmatrix} \sigma_{xx} & \sigma_{xy} & \sigma_{xz} \\ \sigma_{yx} & \sigma_{yy} & \sigma_{yz} \\ \sigma_{zx} & \sigma_{zy} & \sigma_{zz} \end{pmatrix}
$$

$$
= R_z(-\alpha_S)R_x(-\alpha_D)R_z(-\alpha_L) \begin{pmatrix} \sigma_1 & 0 & 0 \\ 0 & \sigma_2 & 0 \\ 0 & 0 & \sigma_3 \end{pmatrix} R_z(\alpha_L)R_x(\alpha_D)R_z(\alpha_S)
$$

where R_x and R_z are elementary rotation matrices around the coordinate axis x and z, respectively.The angles α_S, α_D, α_L are typically called anisotropy strike, dip and slant, respectively.

In this work we investigate the feasibility of use of 2D forward anisotropy modelling to simulate phases over 90° which we observed in field data from the MT survey in South Africa. Using the 2D anisotropy forward modelling algorithm of Pek and Verner (1997) we vary the model parameters in

23. Schmucker-Weidelt-Kolloquium für Elektromagnetische Tiefenforschung,
Heimvolkshochschule am Seddiner See, 28 September - 2 Oktober 2009

88

order to gain a basic understanding of the MT transfer function in presence of anisotropy. First we will give a brief introduction of the survey area and then we will show the results of 2D isotropic inversion and 2D anisotropic forward modelling.

2 Survey area

Within the framework of the German - South African geo-scientific research initiative Inkaba yeAfrica four magnetotelluric (MT) field experiments were conducted along the Agulhas-Karoo Transect in South Africa (Weckmann et al., 2007, Stankiewicz et al., 2008). These transects cross several continental collision zones and their respective units, such as the Cape Fold Belt, the Namaqua Natal Mobile Belt and the Kaapvaal Craton. The MT profile on which we focus in this paper is located in
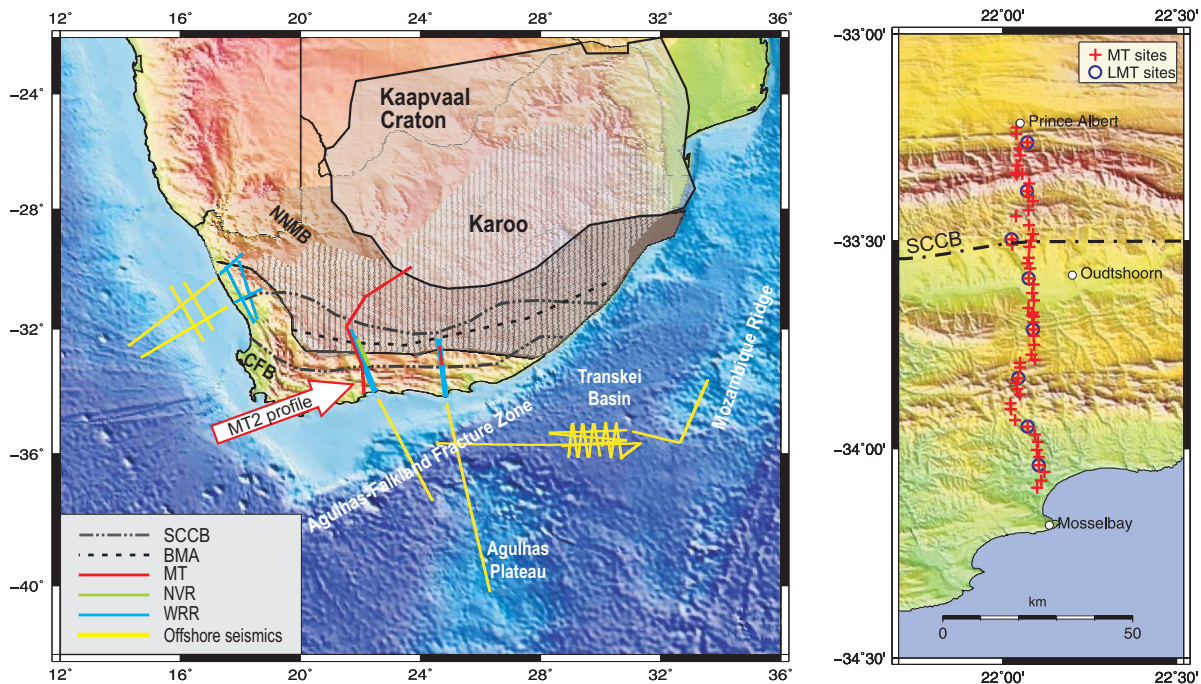

Figure 1: Left: Map of the Agulhas-Karoo Geoscience Transect with MT Profiles (red lines) across Cape Fold Belt , the Namaqua Natal Mobile Belt and the Kaapvaal Craton. Right: The profile MT2 contains 46 broad band MT sites and 8 broad band / long period MT sites. It extends 120 km from Prince Albert in the North to Mosselbay in the South and covers the entire Cape Fold Belt.

the Cape Fold Belt. In total, 54 MT sites were deployed along this 120 km long profile MT 2 (Fig. 1). It extends from Prince Albert in the North to Mosselbay in the South and covers the entire Cape Fold Belt (CFB), its inliers, the Oudtshoorn and the Kaaimans Basins, the Swartberg and the Outeniequa Mountain ranges and several major thrusts and faults.

3 Data and isotropic 2D inversion

Along the profile MT2 we acquired 5-component MT data at all stations in a period range from 0.001s to 1000s using GPS synchronized S.P.A.M. MkIII (Ritter et al., 1998) and CASTLE broadband instrument. Metronix MFS06/06 induction coil magnetometer and non-polarizable Ag/AgCl telluric electrodes were used to record natural magnetic and electric field variations. The data were processed with the EMERALD software package (Ritter et al., 1998) using both robust single site and remote reference techniques. At some sites, for which a suitable reference site was not available and the data were affected by cultural noise (extensive farming), we applied the frequency domain selection scheme after Weckmann et al. (2005) to improve data quality.
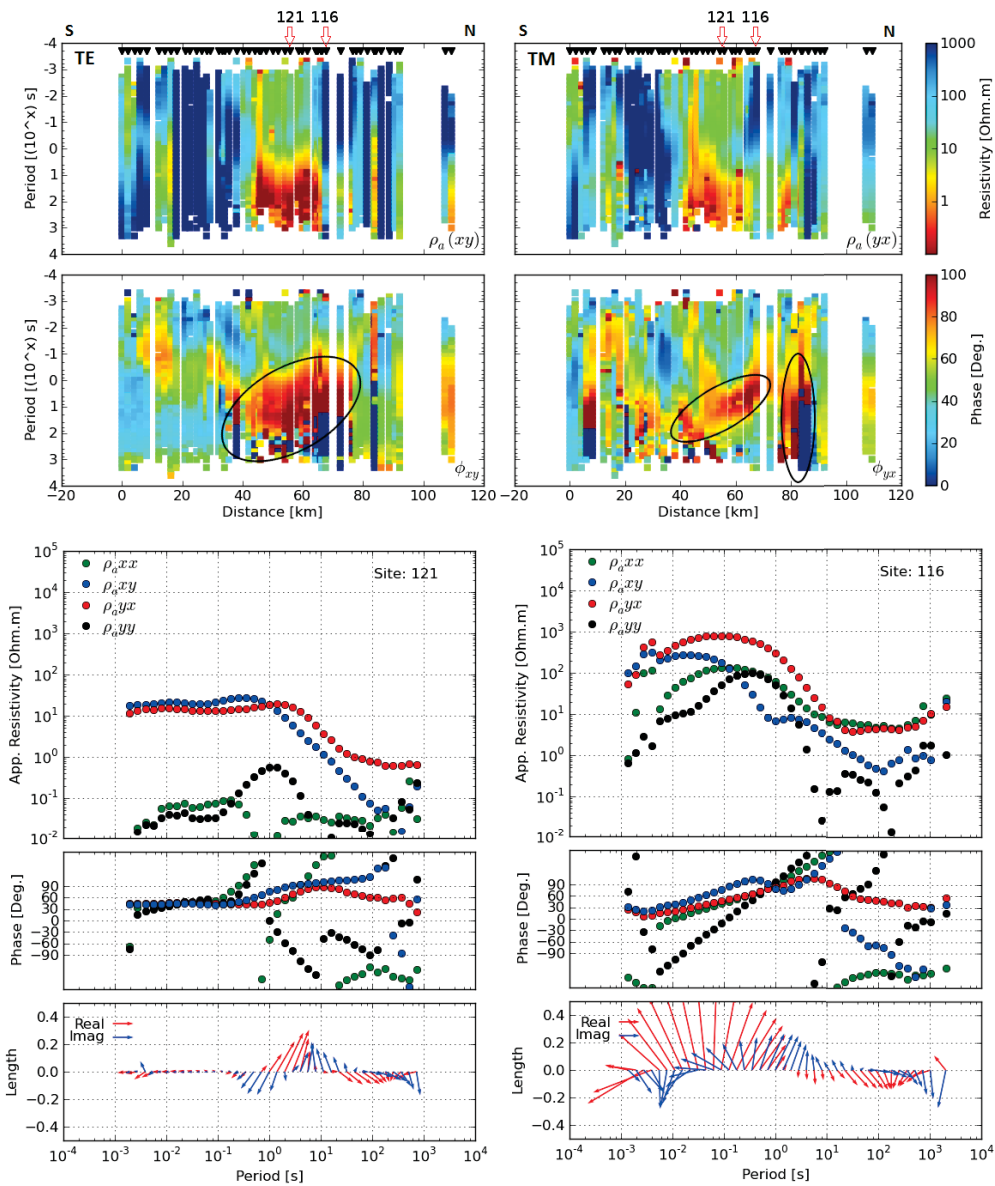
23. Schmucker-Weidelt-Kolloquium für Elektromagnetische Tiefenforschung,
Heimvolkshochschule am Seddiner See, 28 September - 2 Oktober 2009

89

Figure 2: Pseudo-sections of TE and TM mode apparent resistivity and phase (x direction pointing west).We can observe phase values over 90 degrees in the middle of the profile in both TE and TM component (marked with black ellipses in the upper panel). Two exemplary sites (site 121 and site 116) are displayed as apparent resistivity, phase and induction arrows (Wiese convention) over period. The red arrows in the pseudo-sections show the location of the selected sites. We can identify that the phases, (especially in the TE component) leave the first quadrant at a minimum period of 10 s, but typically at longer periods of 100-1000 s.

23. Schmucker-Weidelt-Kolloquium für Elektromagnetische Tiefenforschung,
Heimvolkshochschule am Seddiner See, 28 September - 2 Oktober 2009

90

After data processing, we applied different strike and dimensionality analyses, e.g. the ellipticity analysis after Becken & Burkhardt (2004), obtaining an electromagnetic strike direction of $-90°$, i.e. East-West direction. This is in general compatible with the tectonic grain of the CFB. Furthermore, most of the data seem to be compatible with a 2D interpretation approach. However, in a limited area we observe impedance phases exceeding 90 degrees at long periods. They typically appear in both, TE and TM mode, and persist in either component even if we rotate the coordinate system (Fig. 2).
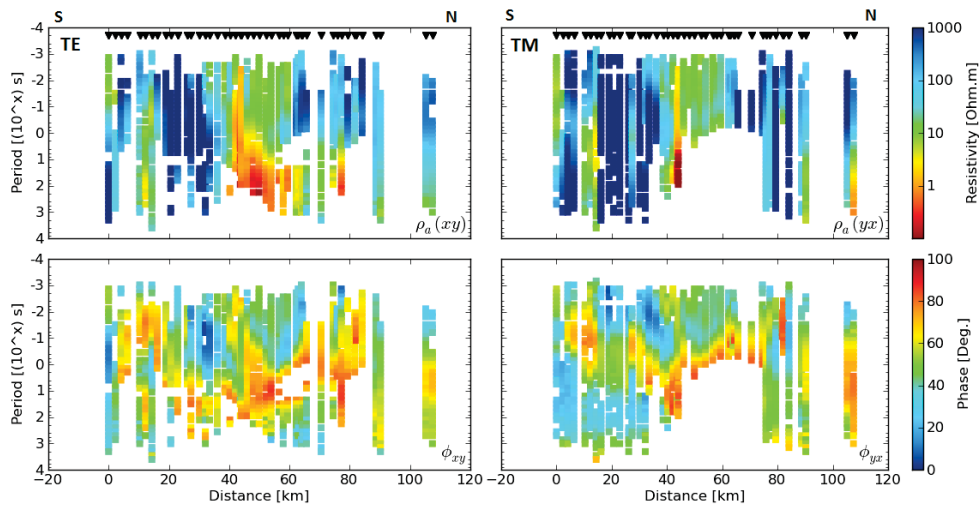

Figure 3: TE and TM mode data used for isotropic 2D inversion. Prior to inversion they were rotated into a common coordinate system according to the geoelectric strike direction of $\approx 90°$ (obtained by strike and phase tensor analysis). Data with phases over $90°$ are discarded from the data base.

For an isotropic 2D inversion approach we use RLM2D (Rodi & Mackie, 2001, implemented in the WinGlink software package). Before starting a 2D inversion we have to make sure that large phase values over $90°$ are excluded as they cannot be fitted by a 2D inversion approach. Figure 3 shows the data which were finally used for 2D inversion. Figure 4 displays our preferred 2D conductivity image of the upper 35 km together with a section of the geological map after Hälbich et al. (1993). The inversion was started from a homogeneous half-space of $100\Omega m$ with $\tau = 10$ using TE and TM component, with intermediate inclusion of the vertical magnetic transfer function. Within the framework of this work, we refrain from interpreting conductivity anomalies in a geological context, but focus on the area where phases over $90°$ occur. One of the most prominent conductivity anomalies is a triangular shaped, highly conductive structure in the middle of the profile. In this area we also observe phases leaving the quadrant. This conductivity anomaly is required by the data which is compatible with a 2D interpretation approach; however, we believe that the phases over $90°$ are caused by some electrically anisotropic structures in this area (in Fig. 4 between black dashed lines). We should also note that the deep part of this area only possesses a very limited resolution (in Fig. 4 marked with semitransparent mask) because most of the data which relates to this part are excluded in order to satisfy the 2D isotropic procedure (see Fig. 3). Similar phase behaviour was explained with crustal anisotropy by Weckmann et al. (2003) and Heise & Pous (2003), where data within old continental collision zones in Namibia and on the Iberian Peninsula, respectively. In both cases the data could be fit by using a shallow and a deeper electrically anisotropic zone with different anisotropy strike.

4   Anisotropic forward modelling

Isotropic 2D inversion is adequate to explain the data in most parts along the profile but it is very unsatisfactory not being able to include phases greater than 90 degrees and thus neglect a substantial amount of data. In order to develop a 2D inversion with spatially constraint anisotropy, resolution tests and synthetic modelling studies are necessary. In a first step towards the constraint anisotropic
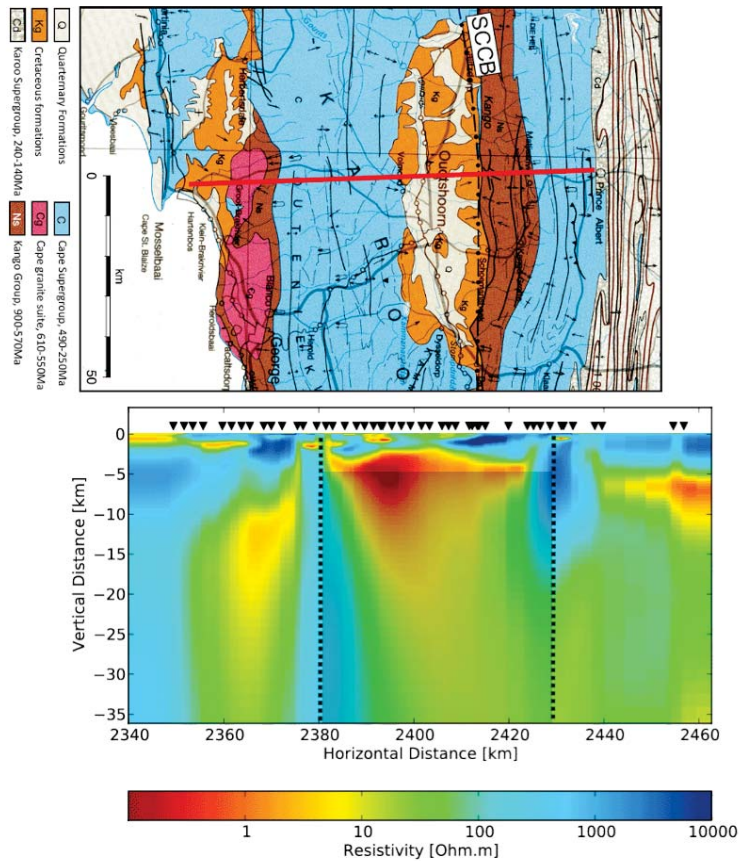
Figure 4: 2D inversion model together with a section from the geological map after Hälbich et al. (1993). The area where we observe phases over 90° is located where the inversion puts a triangular shaped high conductivity anomaly (area between black dashed lines). Zones of limited resolution are also in this area and marked with a semitransparent mask.

inversion we included zones with electrical anisotropy in a 2D isotropic model and calculated its forward responses which aim to understand the anisotropy effect.

4.1 Lateral extension

Pek & Verner (1997) have suggested that a combination of two azimuthal anisotropies with anisotropy strikes perpendicular to each other could produce phases that exceed 90°. Based on the suggestion we study at first a combination of two different anisotropic blocks. The initial model (Fig. 5, left) consists of a $300\,m$ isotropic surface layer with a resistivity of $30\,\Omega m$ and an anisotropic block starting at a depth of $300\,m$ embedded in a medium of $100\,\Omega m$. The principal resistivities of the block are $\sigma_1/\sigma_2/\sigma_3 = 50/0.5/50\,\Omega m$ and the anisotropy strike α_S is $120°$. The block is underlain by an isotropic layer with a resistivity of $15\,\Omega m$. Beneath the isotropic layer a second anisotropic block with $\sigma_1/\sigma_2/\sigma_3 = 30/0.3/30\,\Omega m$ and $\alpha_S = 30°$ (perpendicular to α_S of the first block) is embedded in an isotropic half-space with $100\,\Omega m$. The second, deeper anisotropic block has a lateral extension of $15\,km$ in the first (Fig. 5, left upper panel), and $80\,km$ in the second (Fig. 5, left lower panel) model, respectively.

The forward responses are displayed in figure 5 (right) as apparent resistivities and phases in xy and yx component, respectively. Comparing the responses of both models we see that the phases of yx component (Φ_{yx}) for the second model (Fig. 5, left lower panel) at sites above the first anisotropy block leave the quadrant at a period of $\approx 100\,s$ (Fig. 5, right lower panel), while they are smaller than $90°$ (Fig. 5, right upper panel) for the first model (Fig. 5, left upper panel) with the narrower deep anisotropic block.

23. Schmucker-Weidelt-Kolloquium für Elektromagnetische Tiefenforschung,
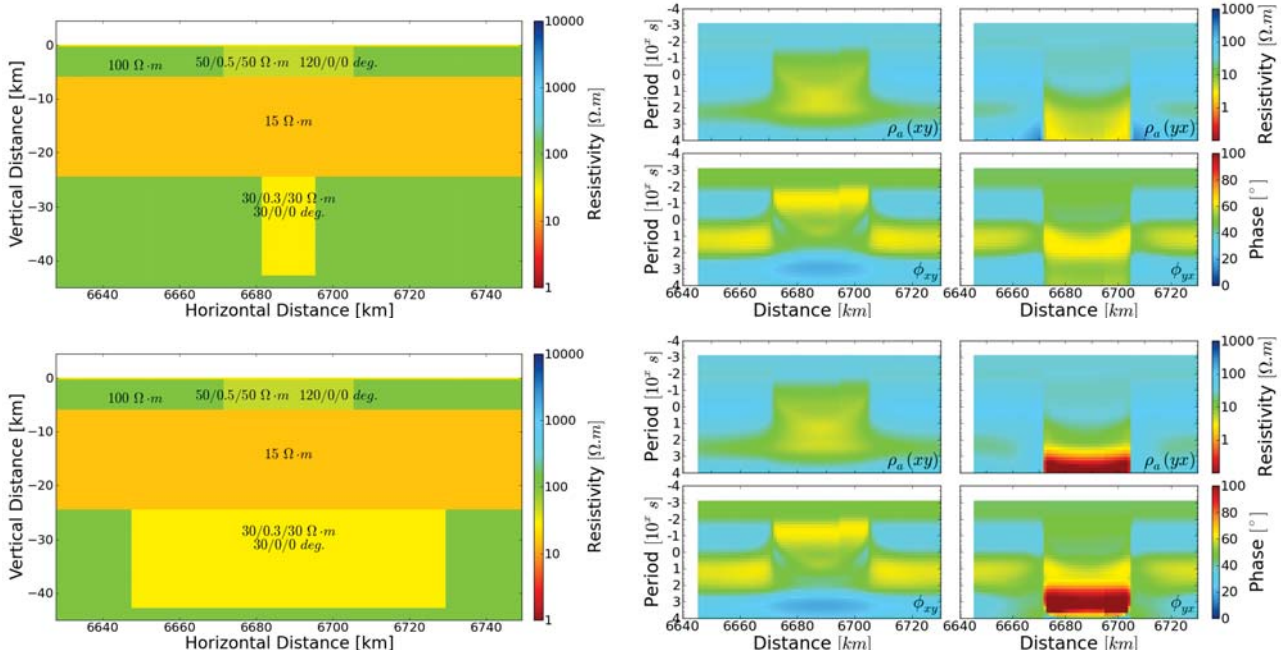Heimvolkshochschule am Seddiner See, 28 September - 2 Oktober 2009

92

Figure 5: Models (left) and their forward responses (right). The models differ only in lateral extension of anisotropy block. The lateral extension of the second block is about $15\,km$ in the first model (left upper panel) and $80\,km$ (left lower panel) in the second model. The major difference in the responses appears in the *yx* component. Phases over $90°$ occur if the lateral extension of the deeper anisotropy block is greater than it of the shallower anisotropy block.

4.2 Depth

In a second step, we used the same anisotropy parameters as described above. The initial model consists of a $300\,m$ isotropic surface layer and a isotropic half-space with resisitivity of $100\,\Omega m$. Two anisotropy blocks are embedded in the half-space. The first block started at depth of $300\,m$ and shaped as a trapezoid. In this attempt we vary the depth of the second block. In the first model (Fig. 6, left upper panel) the second block started at a depth of $1.8\,km$ and in the second model (Fig. 6, left lower panel) started at a depth of $6.8\,km$.

In the forward responses (Fig. 6, right) we see that the phases Φ_{yx} for the second model become larger than $90°$ at periods $> 10\,s$ at sites above the first block, while they for the first model are all smaller than $90°$. In this attempt the second anisotropy block has always sufficiently greater lateral extension than the first anisotropy block, but we only see the phase anomalies by model with anisotropy block in adequate depth. Besides the lateral extension of the anisotropy block, also the depth is one of those key conditions under which phase anomalies appear.

4.3 Rotation angle

In a third test we use a similar model as described above for step two. The model contains a $300\,m$ isotropic surface layer and an isotropic half-space with resisitivity of $100\,\Omega m$. Two anisotropic blocks are embedded in the half-space. The first block starts directly beneath the surface layer and the second block in a depth of $6\,km$. They have the principal resistivities $\sigma_1/\sigma_2/\sigma_3 = 50/0.5/50\,\Omega m$ and $\sigma_1/\sigma_2/\sigma_3 = 30/0.3/30\,\Omega m$, respectively. In this attempt we vary the anisotropy strike angle α_{S1} and α_{S2} for both blocks.

The forward response for the model with $\alpha_{S1} = \alpha_{S2} = 0°$ is displayed in the right upper panel of figure 7. The phases of the *yx* component approach $90°$ for long periods. For $\alpha_{S1} = 60°$ and $\alpha_{S2} = 120°$ (Fig. 7, left lower panel) the *yx* component phases become larger than $90°$ for periods $> 10s$, while they stay below $90°$ for $\alpha_{S1} = 90°$ and $\alpha_{S2} = 120°$ (Fig. 7, right lower panel). Comparing the three examples, we see that model with different combination of strike angle in both shallow and
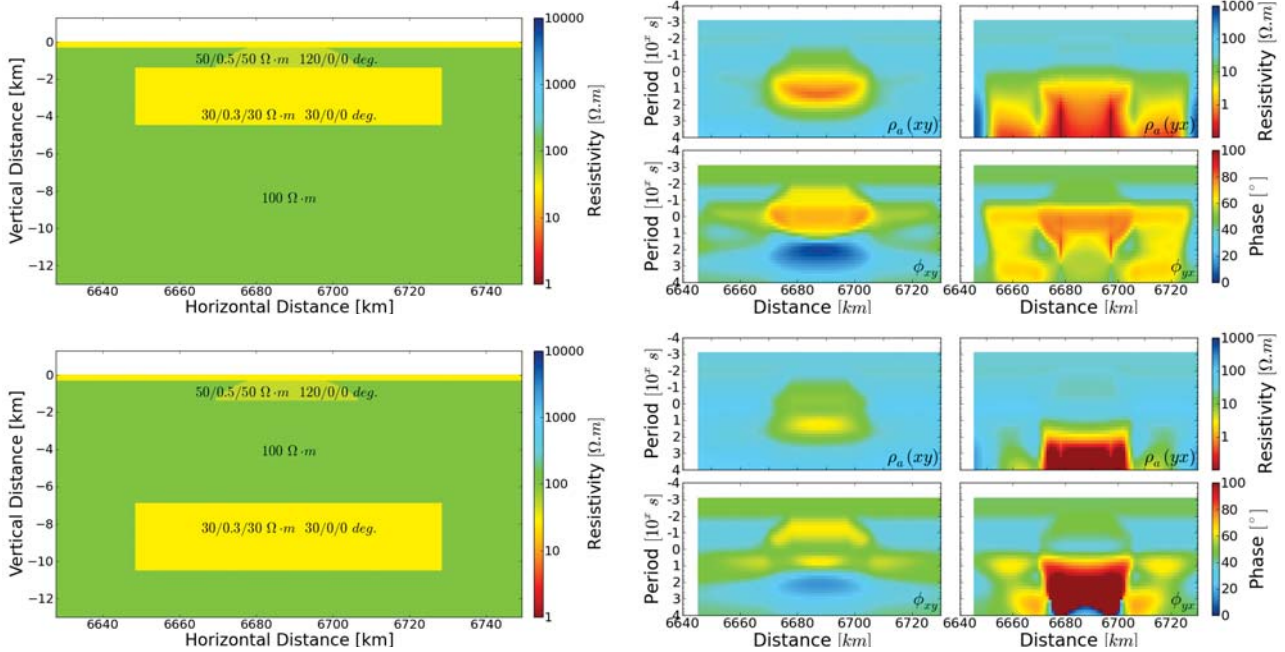
Figure 6: Models (left) and their forward responses (right). The models differ by depth of the second anisotropy block. In the first model (left upper panel) the second block starts in a depth of $1.8\,km$ and in the second model (left lower panel) the block starts in a depth of $6.8\,km$. The phases of yx component for the model with the deeper anisotropic block become larger than $90°$ at periods $> 10\,s$ at sites above the first block. For the model with the shallower block all phases are smaller than $90°$.
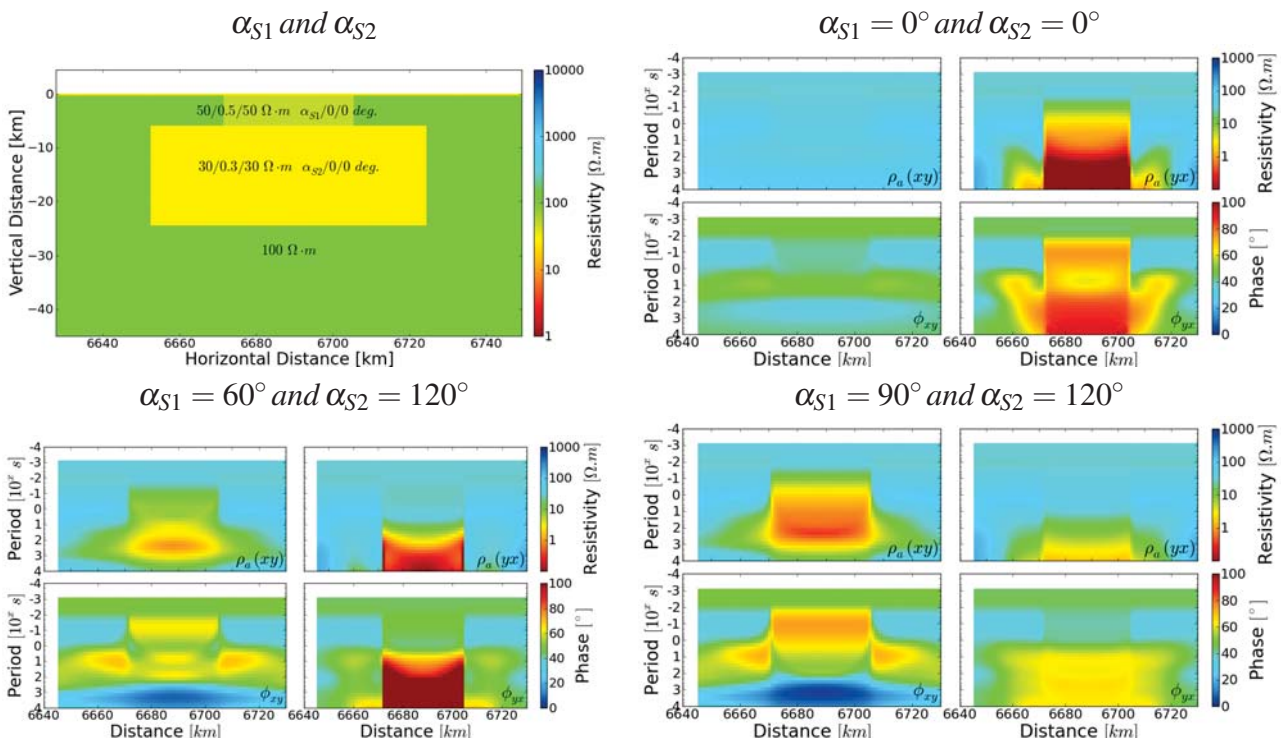

Figure 7: Model (left upper panel) and its forward responses with different anisotropy strike angles. The model contains the same surface layer, background medium and resistivities for both anisotropic blocks as the models in fig. 6. We vary the strike angles α_{S1} and α_{S2} for the shallow and the deep block (left upper panel). The forward responses are displayed as apparent resistivities and phases in xy and yx component.

23. Schmucker-Weidelt-Kolloquium für Elektromagnetische Tiefenforschung,
Heimvolkshochschule am Seddiner See, 28 September - 2 Oktober 2009

94

deep blocks produce forward responses with pronounced difference. This can be observed not only in yx component ($\rho_a(yx)$ and Φ_{yx}) but also in xy component ($\rho_a(xy)$ and Φ_{xy}). A possible explanation is that a change of strike angle forces the current flow to change its preferred direction from the shallow to the deep block. According to this fact we may conclude that the anisotropy strike angle influences forward responses significantly and phase greater than $90°$ will appear if the strike angle of both blocks differ by an adequate amount.

5 Conclusions

Phases greater than $90°$ can only be modelled by a combination of a deep and a shallow anisotropic block. We varied several model parameters to study the changes in forward responses. For our models we can conclude that phases out of the first quadrant occur when: (i) the anisotropy ratio ($\sigma_{max}/\sigma_{min}$) is high (for both blocks); (ii) the deep anisotropic block has a much larger lateral extension than the shallow block; (iii) the deep anisotropic block is located in greater depth; (iv) the angles of anisotropy of both blocks differ by a considerable amount. In our models the difference should be at least $45°$ so that the preferred direction of current flow changes significantly from the shallow to the deep block.

References

Becken, M., & Burkhardt, H. (2004). An ellipticity criterion in magnetotelluric tensor analysis. *Geophys. J. Int.*, *159*, 69–82.

Eisel, M., & Haak, V. (1999). Macro-anisotropy os the electrical conductivity of the crust: a magnetotelluric study from the German continental Deep Drilling site (KTB). *Geophys. J. Int.*, *136*, 109–122.

Hälbich, I. (1993). Cape Fold Belt – Agulhas Bank Transect across Gondwana suture, southern Africa. *Geosci. Transect*, *9*, 18 pp. AGU, Washington, D. C.

Heise, W., & Pous, J. (2003). Anomalous phases exceeding $90°$ in magnetotellurics: anisotropic model studies and a field example. *Geophys. J. Int.*, *155*, 308–318.

Kellett, R. L., Mareschal, M., & Kurtz, R. D. (1992). A model of lower crustal electrical anisotropy for the Pontiac Subprovince of the Canadian Shield. *Geophys. J. Int.*, *111*, 141–150.

Mareschal, M., Kellett, R. L., Kurtz, R. D., Ludden, J. N., Ji, S., & Bailey, R. C. (1995). Archaean cratonic roots, mantle shear zones and deep electrical anisotropy. *Nature*, *375*, 134–137.

O'Brien, D. P., & Morrison, H. F. (1967). Electromagnetic fields in an N-layer anisotropic half space. *Geophysics*, *32*, 668–677.

Pek, J., & Verner, T. (1997). Finite-difference modelling of magneto-telluric fields in two-dimensional anisotropic media. *Geophys. J. Int.*, *128*, 505–521.

Reddy, I. K., & Rankin, D. (1975). Magnetotelluric response of lateerally inhomogeneous and anisotropic media. *Geophysics*, *40*, 1035–1045.

Ritter, O., Junge, A., & Dawes, G. J. K. (1998). New equipment and processing for magnetotelluric remote reference observations. *Geophys. J. Int.*, *132*, 535–548.

Rodi, W., & Mackie, R. L. (2001). Nonlinear conjugate gradients algorithm for 2-d magnetotelluric inversion. *Geophysics*, *66*, 174–187.

Stankiewicz, J., Ryberg, T., Schulzw, A., Lindeque, A., Weber, M., & de Wit, M. (2007). Initial results from wide-angle seismic refraction lines in the southern Cape. *South African Journal of Geology*, *110*, 407–418.

Weckmann, U., Jung, A., Branch, T., & Ritter, O. (2007). Comparison of electrical conductivity structures and 2D magnetic modelling along two profiles crossing the Beattie Magnetic Anomaly, South Africa. *South African Journal of Geology*, *110*, 449–464.

Weckmann, U., Magunia, A., & Ritter, O. (2005). Effective noise separation for magnetic single site data processing using a frequency domain selection scheme. *Geophys. J. Int.*, *161*, 635–652.

Weckmann, U., Ritter, O., & Haak, V. (2003). A magnetotelluric study of the damara belt in namibia – 2. MT phases over 90° reveal the internal structure of the Waterberg Fault/Omaruru Lineament. *Phys. Earth Planet. Inter.*, *138(2)*, 91–112.